

The Effect of Massive Neutrinos on the Halo Spin Flip Phenomenon

Jounghun Lee¹, Noam I Libeskind^{2,3}, Suho Ryu¹

ABSTRACT

The halo spin flip refers to the phenomenon that the spin axes of dark matter halos with masses above a certain threshold tend to be preferentially aligned perpendicular to the hosting large-scale filaments, while low-mass halos tend to have their spin axes aligned parallel to such structures. Extensive work has so far been conducted to understand this phenomenon under the assumption of cold dark matter and suggested that its origin should be closely related to the nonlinear evolution of the halo angular momentum in the anisotropic cosmic web. We present, for the first time, a numerical examination of this phenomenon assuming the presence of massive neutrinos, finding a clear and robust dependence of the threshold mass for the spin flip on the total neutrino mass. Our physical explanation is that the presence of more massive neutrinos retard the nonlinear evolution of the cosmic web, which in turn allows the halo spin vectors to better retain their memories of the initial tidal interactions in the nonlinear regime. Our finding implies that the statistical alignment of halo spins with the large-scale structures can be in principle used as a probe of the total neutrino mass.

Subject headings: Unified Astronomy Thesaurus concepts: Large-scale structure of the universe (902); Cosmological models (337)

1. Introduction

The total mass of neutrino species, $\sum m_\nu$, whose non-zero value was confirmed by the detection of neutrino flavor oscillations (for a comprehensive review, see Gonzalez-Garcia &

¹Department of Physics and Astronomy, Seoul National University, Seoul 08826, Republic of Korea
jounghun@astro.snu.ac.kr, ryu@snu.ac.kr

²Leibniz-Institut für Astrophysik Potsdam (AIP), An der Sternwarte 16, 14482 Potsdam, Germany
noam@aip.cn.kr

³University of Lyon, UCB Lyon-1/CNRS/IN2P3, IPN Lyon, France

Maltoni 2008) is of vital importance not only in particle physics but also in cosmology. In the former, the non-zero value of $\sum m_\nu$ is the most conclusive counter proof against the standard model of particle physics (Gonzalez-Garcia & Maltoni 2008). In the latter, the presence of massive neutrinos has an effect of suppressing the growth of the matter densities on a scale determined by $\sum m_\nu$ due to their ability to free stream out of gravitational potential wells (Bond et al. 1980; Pogosyan & Starobinsky 1993, 1995). In fact, a close coaction of particle physics with cosmology is required to constrain $\sum m_\nu$, since laboratory experiments have a capacity of putting only a lower limit on $\sum m_\nu$ (Gonzalez-Garcia & Maltoni 2008). The optimal way to determine the upper limit of $\sum m_\nu$, which is most crucial to the physical understanding of their properties, is to resort to the cosmological observables that sensitively depend on $\sum m_\nu$ (for a review, see Lesgourgues & Pastor 2006).

The previous works that attempted to probe $\sum m_\nu$ by using such cosmological observables as the linear density power spectra, abundance of galaxy clusters and etc., focused mainly on the suppressing effect of massive neutrinos on the amplitudes of the matter densities (e.g., see Lesgourgues & Pastor 2006, 2012, 2014, and references therein). However, it can be speculated that the presence of massive neutrinos would affect not only the amplitudes of the matter densities but also the eigen directions of the tidal fields defined as the second derivative of the gravitational potentials and used to quantify the cosmic web (Bond et al. 1996). A cosmological observable that is susceptible to the effect of massive neutrinos on the tidal eigen directions, if existent and found, may provide a complementary probe of $\sum m_\nu$.

Here, we attempt to identify one such probe by investigating how the presence of massive neutrinos affects threshold mass at which the preferred directions in the spin orientations of dark matter (DM) halos "flip" from parallel to perpendicular to the elongated axes of the surrounding filaments, which is often dubbed the "halo spin flip" phenomenon (Codis et al. 2012). The occurrence of the halo spin flip was first witnessed in numerical works based on N-body simulations which investigated the orientations of halo spins with respect to surrounding large-scale structures as defined by the eigenvectors of the local tidal tensors and found that the spin vectors of the galactic halos having masses lower (higher) than a certain threshold were oriented parallel (perpendicular) to the directions of minimum compression (e.g., Aragón-Calvo et al. 2007; Hahn et al. 2007b; Paz et al. 2008; Codis et al. 2012; Trowland et al. 2013; Libeskind et al. 2013; Aragon-Calvo & Yang 2014; Dubois et al. 2014; Forero-Romero et al. 2014; Codis et al. 2015a,b, 2018; Ganeshaiah Veena et al. 2018; Wang et al. 2018; Lee 2019; Kraljic et al. 2020). The galaxies resolved in the cosmological hydrodynamic simulations were shown to exhibit weaker signals of the mass-dependent spin flip (Dubois et al. 2014; Codis et al. 2018; Ganeshaiah Veena et al. 2019; Kraljic et al. 2020) than the DM halos, which were attributed to more complicated merging processes of the galaxies and baryonic effects.

What observations found was a signal of the morphology dependent flip of the galaxy spins. While the minor axes of the early-type galaxies tend to be aligned with the directions perpendicular to the host filaments, the spin directions of the late-type galaxies exhibit alignments with the directions parallel to the filaments. (see also Tempel & Libeskind 2013; Tempel et al. 2013; Pahwa et al. 2016; Hirv et al. 2017). Very recently, the first observational evidence for the stellar mass dependent flip of the galaxy spins was reported by Welker et al. (2020) who utilized the data from the Sydney-Australian Astronomical Observatory Multi-object Integral Field Spectrograph surveys (Bryant et al. 2015) (see also Blue Bird et al. 2019).

A multitude of scenarios has been put forth to explain what causes the occurrence of the spin flip and why it occurs at a particular threshold mass (Aragon-Calvo & Yang 2014; Welker et al. 2014; Wang & Kang 2018; Codis et al. 2015b). Although the origin and underlying mechanism has yet to be fully understood, it is now generally accepted that the evolutionary process in the cosmic web is largely responsible for the occurrence of the halo spin flip (Aragon-Calvo & Yang 2014; Welker et al. 2014; Wang & Kang 2018; Codis et al. 2015b). Meanwhile, a recent numerical analysis hinted that the presence of massive neutrinos affects the degree of the anisotropy of the cosmic web (Ryu & Lee 2020). Given this hint and recalling that the strength and tendency of the tidally induced spin alignments of DM halos depends sensitively on the anisotropy of the surrounding web environments (Hahn et al. 2007a; Libeskind et al. 2013; Lee 2019), we propose a hypothesis that the threshold mass for the halo spin flip may also depend on $\sum m_\nu$.

The linear tidal field acts on the spin axes of the proto-galactic halos to be aligned with its second eigen direction (White 1984; Lee & Pen 2000, 2001). If the galactic halos became decoupled from the surroundings after the gravitational collapse, their spin directions would retain well the initially induced alignments. In reality, the galactic halos located in the cosmic web usually do not become completely decoupled from the surroundings but rather prone to their tidal influences. Undergoing the nonlinear evolution, the filamentary cosmic web itself becomes thicker and more intricate, whose tidal influence would have an effect of diminishing the strengths of the initially induced alignments of the halo spin directions (e.g., Hahn et al. 2010; Aragon-Calvo & Yang 2014).

The lower-mass galactic halos which form earlier and have sizes smaller than the thickness of the filaments would be more vulnerable to the effect of the nonlinearly evolved filamentary cosmic web than the higher-mass ones (Aragon-Calvo & Yang 2014). The threshold mass for the spin flip corresponds to the mass scale below which the initially induced alignments of the halo spin axes are overwhelmed by the effect of the nonlinearly evolved cosmic web. The faster the cosmic web evolves, the halo spin flip would occur at a higher mass

scale. In the presence of massive neutrinos, the suppressed small-scale powers would retard the nonlinear evolution of the cosmic web, which in consequence would lead the spin flip to occur at a lower mass scale.

Our goal here is to test this hypothesis against N-body simulations performed for the $\nu\Lambda$ CDM models (neutrinos + cosmological constant Λ + cold DM) whose initial conditions are different only in $\sum m_\nu$. Instead of identifying filamentary structures from the spatial distributions of DM halos, we will directly reconstruct the tidal fields from the spatial distributions of the DM particles. Measuring the alignments between the spin axes of DM halos and the tidal eigenvectors, we will explore if and at what mass scale the halo spin directions flip from the second to the third tidal eigenvectors (corresponding to the perpendicular to the parallel directions to the filaments).

Throughout this Paper, we will use the following notations to denote the relevant quantities: $\mathbf{J} = (J_i)$ (spin vector of a DM halo), $\hat{\mathbf{J}} = (\hat{J}_i)$ (direction of \mathbf{J}), $\mathbf{T} = (T_{ij})$ (smoothed tidal shear tensor), $\hat{\mathbf{T}} = (\hat{T}_{ij})$ (traceless version of \mathbf{T} rescaled by $|\mathbf{T}|$), $\{\lambda_i\}_{i=1}^3$ (eigenvalues of \mathbf{T} in a decreasing order), $\{\mathbf{e}_i\}_{i=1}^3$ (eigenvectors of \mathbf{T} corresponding to $\{\lambda_i\}_{i=1}^3$), $\{\hat{\mathbf{e}}_i\}_{i=1}^3$ (eigenvectors of $\hat{\mathbf{T}}$), $\{\hat{\lambda}_i\}_{i=1}^3$ (eigenvalues of $\hat{\mathbf{T}}$), R_f (smoothing scale), M_h (halo mass), M_{flip} (threshold mass at which the strength of the $\hat{\mathbf{J}}\text{-}\hat{\mathbf{e}}_2$ alignment becomes comparable to that of the $\hat{\mathbf{J}}\text{-}\hat{\mathbf{e}}_3$ alignment), and $p(\cos\theta_i)$ (probability density of the cosine of the angle, θ_i , between $\hat{\mathbf{J}}$ and $\hat{\mathbf{e}}_i$ for $i \in \{1, 2, 3\}$).

2. Data and Analysis

Our numerical investigation relies entirely on the publicly available data from the Cosmological Massive Neutrino Simulations (**MassiveNuS**), which is a suite of DM only N -body simulations performed on a cosmological box of comoving $512 h^{-1}\text{Mpc}$ aside, containing 1024^3 particles with individual mass of $10^{10} h^{-1} M_\odot$ (Liu et al. 2018). A total of 101 $\nu\Lambda$ CDM models having unequal initial conditions were adopted by the **MassiveNuS** as the background cosmologies, among which three models, with $\sum m_\nu = 0.0, 0.1$ and 0.6 eV , are selected for our analysis since they share the same initial conditions other than $\sum m_\nu$. The analytic linear response approximation was employed by Liu et al. (2018) to include the massive neutrinos in the background for the **MassiveNuS**.

The **MassiveNuS** also provides a catalog of bound objects identified by the Rockstar algorithm (Behroozi et al. 2013), which includes not only the distinct halos but also their substructures. Eliminating the substructures from the catalog, we select the distinct galactic halos with masses in the logarithmic range of $11.8 \leq \log(M_h/h^{-1}M_\odot) < 13$, for each of the

three selected models. Table 1 lists the values of the key cosmological parameters and the numbers of the distinct galactic halos (N_g) for the three selected models. Note that although the three models share the same value of the primordial power spectrum amplitude (A_s), they differ from one another in the value of the rms density fluctuation within a top-hat radius of $8 h^{-1}\text{Mpc}$ (σ_8).

Dividing the simulation box into a grid of 256^3 cells, we determine the raw density contrast, $\delta(\mathbf{x})$, at the location of each grid cell, \mathbf{x} , by applying a cloud-in-cell algorithm to the particle distribution at $z = 0$. Performing the Fast Fourier Transformation (FFT) of $\delta(\mathbf{x})$, we obtain its Fourier amplitude, $\tilde{\delta}(\mathbf{k})$, at each Fourier-space wave vector, $\mathbf{k} = (k\hat{k}_i)$. An inverse FFT of $\tilde{T}_{ij}(\mathbf{k}) \equiv \hat{k}_i\hat{k}_j\tilde{\delta}(\mathbf{k}) \exp[-k^2 R_f^2/2]$ returns, $T_{ij}(\mathbf{x})$ with $i, j \in \{1, 2, 3\}$, the tidal field smoothed by a Gaussian window function on the scale of R_f .

Locating the grid point, \mathbf{x}_h , where each galactic halo resides, we calculate $\hat{\mathbf{T}}(\mathbf{x}_h)$ by subtracting the trace from $\mathbf{T}(\mathbf{x}_h)$ and rescaling it by its magnitude. Finding $\{\hat{\lambda}\}_{i=1}^3$ and $\{\hat{\mathbf{e}}\}_{i=1}^3$ at the location of each galactic halo through a similarity transformation of $\hat{\mathbf{T}}(\mathbf{x}_h)$, we compute the projection of $\hat{\mathbf{J}}$ onto each tidal eigenvector as $\cos\theta_i = |\hat{\mathbf{J}} \cdot \hat{\mathbf{e}}_i|$. Splitting the logarithmic mass range, $11.8 \leq \log M_h < 13$, into six differential bins, we determine the probability density distribution, $p(\cos\theta_i)$, as well as the ensemble average at each mass bin. If $\hat{\mathbf{J}}$ is not aligned with $\hat{\mathbf{e}}_i$, we expect a uniform distribution of $p(\cos\theta_i) = 1$. If $\hat{\mathbf{J}}$ is aligned with the direction parallel (perpendicular) to $\hat{\mathbf{e}}_i$, we expect $p(\cos\theta_i)$ to be an increasing (decreasing) function of $\cos\theta_i$, yielding $\langle\cos\theta_i\rangle > 0.5$ ($\langle\cos\theta_i\rangle < 0.5$). The linear tidal torque theory (TTT) (White 1984) predicts $\langle\cos\theta_2\rangle > 0.5$, $\langle\cos\theta_3\rangle \sim 0.5$ and $\langle\cos\theta_1\rangle < 0.5$ in the proto-galactic stages, regardless of M_h (Lee & Pen 2000).

Figure 1 plots $\langle\cos\theta_1\rangle$ (green lines), $\langle\cos\theta_2\rangle$ (red lines) and $\langle\cos\theta_3\rangle$ (blue lines) at the six logarithmic mass bins for the two cases of $\sum m_\nu = 0.0\text{eV}$ (top panel) and $\sum m_\nu = 0.6\text{eV}$ (bottom panel). For this plot, we set R_f at $5 h^{-1}\text{Mpc}$, leaving out the results for the case of $\sum m_\nu = 0.1\text{eV}$, which turns out to be almost the same as those for the case of $\sum m_\nu = 0.0\text{eV}$. The errors are calculated as one standard deviation in the mean value as $[(\langle\cos^2\theta_i\rangle - \langle\cos\theta_i\rangle^2)/(n_g - 1)]^{1/2}$, where n_g denotes the number of the distinct DM halos in each bin. As can be seen, the two $\nu\Lambda\text{CDM}$ models yield a similar trend. As M_h decreases, the value of $\langle\cos\theta_2\rangle$ almost monotonically diminishes down to 0.5, while the values of $\langle\cos\theta_1\rangle$ and $\langle\cos\theta_3\rangle$ mildly increase. In the entire mass range of $11.8 \leq \log M_h < 13$, the value of $\langle\cos\theta_2\rangle$ ($\langle\cos\theta_1\rangle$) remains higher (lower) than 0.5. Whereas, the value of $(\langle\cos\theta_3\rangle - 0.5)$ switches its sign midway, which leads $\langle\cos\theta_3\rangle \geq \langle\cos\theta_2\rangle$ in the mass range below a certain threshold. The two $\nu\Lambda\text{CDM}$ differ from each other in the rate at which $\langle\cos\theta_3\rangle$ increases with the decrement of M_h and in the value of the threshold mass at which $\langle\cos\theta_3\rangle \sim \langle\cos\theta_2\rangle$.

We define, M_{flip} , as the threshold mass at which the strength of the *parallel* alignment

between $\hat{\mathbf{J}}$ and $\hat{\mathbf{e}}_3$ becomes comparable to that between $\hat{\mathbf{J}}$ and $\hat{\mathbf{e}}_2$. To find M_{flip} for the two $\nu\Lambda\text{CDM}$ models, we statistically evaluate the similarity between the strengths of the $\hat{\mathbf{J}}\text{-}\hat{\mathbf{e}}_2$ and $\hat{\mathbf{J}}\text{-}\hat{\mathbf{e}}_3$ alignments at each bin. Instead of comparing simply $\langle \cos \theta_3 \rangle$ with $\langle \cos \theta_2 \rangle$, we take a more rigorous approach, performing the KolmogorovSmirnov (KS) test of the null hypothesis of $p(\cos \theta_2) \sim p(\cos \theta_3)$. If the spin flip occur at a certain mass bin, then the confidence level for the rejection of this null hypothesis by the KS test would drop below 99.9%.

It is worth mentioning here the advantage of defining M_{flip} as a threshold mass at which $p(\cos \theta_3) \sim p(\cos \theta_2)$ and $\langle \cos \theta_3 \rangle \geq 0.5$. The previous works conventionally defined M_{flip} as the threshold mass at which $\langle \cos \theta_3 \rangle \geq 0.5$. However, this conventional definition of M_{flip} does not take into proper account the possibility that $\hat{\mathbf{J}}$ can be simultaneously aligned with both of $\hat{\mathbf{e}}_2$ and $\hat{\mathbf{e}}_3$ (i.e., $\langle \cos \theta_2 \rangle > 0.5$ and $\langle \cos \theta_3 \rangle > 0.5$). If the $\hat{\mathbf{J}}\text{-}\hat{\mathbf{e}}_2$ alignment is stronger than the $\hat{\mathbf{J}}\text{-}\hat{\mathbf{e}}_3$ alignment (i.e., $\langle \cos \theta_2 \rangle > \langle \cos \theta_3 \rangle > 0.5$), then $\hat{\mathbf{J}}$ would appear to be aligned perpendicular to the elongated axes of the filaments (i.e., the directions of minimum compression) in spite of $\langle \cos \theta_3 \rangle > 0.5$. The neglect of this possibility would result in a spurious value of M_{flip} . Suppose that $\langle \cos \theta_2 \rangle > \langle \cos \theta_3 \rangle > 0.5$ at a given mass M_h . According to our definition, we would properly conclude $M_{\text{flip}} < M_h$, while the conventional method based only on $\langle \cos \theta_3 \rangle$ would spuriously claim $M_{\text{flip}} > M_h$.

Two cumulative distributions, $P(\cos \theta_2 < \cos \theta)$ and $P(\cos \theta_3 < \cos \theta)$ defined as $P(\cos \theta_i < \cos \theta) \equiv \int_0^{\cos \theta} d \cos \theta'_i p(\cos \theta'_i)$, are determined. If there is no alignment between $\hat{\mathbf{J}}$ and $\hat{\mathbf{e}}_i$, we expect $P(\cos \theta_i < \cos \theta) = \cos \theta$. The alignment of $\hat{\mathbf{J}}$ with the parallel and perpendicular directions of $\hat{\mathbf{e}}_i$ would yield $P(\cos \theta_i < \cos \theta) < \cos \theta$ and $P(\cos \theta_i < \cos \theta) > \cos \theta$, respectively. We calculate the maximum distance between the two distributions at each mass bin as

$$D_{2,3} = \max |P(\cos \theta_3 < \cos \theta) - P(\cos \theta_2 < \cos \theta)|, \quad (1)$$

and multiply $D_{2,3}$ by $\sqrt{n_g/2}$ where n_g is the number of the galactic halos at a given mass bin. If this quantity, $\sqrt{n_g/2} D_{2,3}$, is larger than 1.949, then the null hypothesis is rejected at the confidence level higher than 99.9%.

The six panels of Figure 2 show $\cos \theta - P(\cos \theta_2 < \cos \theta)$ (red lines) and $\cos \theta - P(\cos \theta_3 < \cos \theta)$ (blue lines) for the case of $\sum m_\nu = 0.0 \text{ eV}$ at the six logarithmic mass bins: $12.8 \leq \log M_h < 13$ (top left panel), $12.6 \leq \log M_h < 12.8$ (top right panel), $12.4 \leq \log M_h < 12.6$ (middle left panel), $12.2 \leq \log M_h < 12.4$ (middle right panel), $12.0 \leq \log M_h < 12.2$ (bottom left panel), and $11.8 \leq \log M_h < 12$ (bottom right panel). The KS test rejects the null hypothesis at the confidence levels higher than 99.9% in the first three bins but only at the 90% confidence level at the fourth mass bin (middle right panel) where $\langle \cos \theta_3 \rangle > 0.5$, indicating the occurrence of the spin flip in the fourth mass bin, i.e., $\log M_{\text{flip}} \sim (12.3 \pm 0.1)$ for the case of $\sum m_\nu = 0.0 \text{ eV}$. Figure 3 shows the same as Figure 2 but for the case of

$\sum m_\nu = 0.6 \text{ eV}$, revealing that the null hypothesis is rejected at the 99.9% confidence level in the fourth mass bin unlike the case of $\sum m_\nu = 0.0 \text{ eV}$. The drop of the confidence level below 99.9% occurs at the fifth mass bin (bottom left panel) where $\langle \cos \theta_3 \rangle > 0.5$, indicating $\log M_{\text{flip}} \sim (12.1 \pm 0.1)$ for the case of $\sum m_\nu = 0.6 \text{ eV}$. These results imply that the presence of more massive neutrinos has an effect of rendering the spin flip to occur at lower mass scales.

To see whether or not our detection of the dependence of M_{flip} on $\sum m_\nu$ is robust against the variation of R_f , we smooth \mathbf{T} on the larger scale of $R_f = 10 h^{-1} \text{Mpc}$ and repeat the whole process, the results of which are displayed in Figures 4-6. As can be seen, the increase of R_f weakens the overall $\hat{\mathbf{J}}\text{-}\hat{\mathbf{e}}_i$ alignments, which is consistent with the previous works (e.g., Tempel & Libeskind 2013; Lee 2019). It also leads the spin flip phenomenon to occur at a larger mass bin for both of the $\nu\Lambda\text{CDM}$ models. The drop of the confidence level for the rejection of the null hypothesis below 99.9% is found in the third mass bin of $\log M_{\text{flip}} \sim (12.5 \pm 0.1)$ for the case of $\sum m_\nu = 0.0 \text{ eV}$ and in the fourth mass bin of $\log M_{\text{flip}} \sim (12.3 \pm 0.1)$ for the case of $\sum m_\nu = 0.6 \text{ eV}$. This result confirms that M_{flip} depends on $\sum m_\nu$, regardless of R_f .

Since the spin-flip phenomenon was known to be the most prominent in the filamentary environment (Aragón-Calvo et al. 2007; Codis et al. 2012; Ganeshaiah Veena et al. 2018; Lee 2019; Kraljic et al. 2020), we refollow the whole procedure but with only those halos located in the grid points at which the filament condition of $\lambda_2 \geq 0, \lambda_3 < 0$ is satisfied (Hahn et al. 2007a). Figures 7-9 plot the same as Figures 1-3, respectively, but using only the filament halos. The condition for the occurrence of the spin flip, the drop of the confidence level for the rejection of the null hypothesis below 99.9% is found to be satisfied at $\log M_{\text{flip}} = (12.3 \pm 0.1)$ and $\log M_{\text{flip}} = (11.9 \pm 0.1)$ for the cases of $\sum m_\nu = 0.0 \text{ eV}$ and $\sum m_\nu = 0.6 \text{ eV}$, respectively. The filament halos exhibit a larger difference in M_{flip} between the two $\nu\Lambda\text{CDM}$ models, which implies that the filaments are indeed optimal environment for the investigation of the $\sum m_\nu$ -dependence of M_{flip} .

In a similar manner, we also examine if the $\sum m_\nu$ -dependence of M_{flip} can be found in the sheets ($\lambda_1 > 0, \lambda_2 < 0$) (Hahn et al. 2007a), the results of which are shown in Figure 10. As can be seen, in the sheets on the scale of $R_f = 5 h^{-1} \text{Mpc}$, we find no occurrence of the halo spin flips since $\langle \cos \theta_2 \rangle > \langle \cos \theta_3 \rangle \sim 0.5$ in the whole mass range for both of the $\nu\Lambda\text{CDM}$ cosmologies. Note also that in the sheet environments on the scale $R_f = 5 h^{-1} \text{Mpc}$, the intrinsic spin alignments of galactic halos with the tidal eigenvectors -for both of the models follow very well the predictions of the linear TTT, which is consistent with the observational result of Lee et al. (2018). No signal of the $\sum m_\nu$ -dependence of M_{flip} is found even when R_f varies from $5 h^{-1} \text{Mpc}$ to $10 h^{-1} \text{Mpc}$.

For the knot halos ($\lambda_3 > 0$), we detect a clear signal of the $\sum m_\nu$ -dependence of M_{flip} on

the scale of $R_f = 2 h^{-1}\text{Mpc}$, as shown in Figure 11-13. The spin flips are found to occur at $\log M_{\text{flip}} = 12.7 \pm 0.1$ and 12.5 ± 0.1 for the cases of $\sum m_\nu = 0.0 \text{ eV}$ and 0.6 eV , respectively. The results from the knots on the larger scales of $R_f = 5 h^{-1}\text{Mpc}$ and $10 h^{-1}\text{Mpc}$ as well as from the voids are found to carry large uncertainties due to poor number statistics and thus omitted here.

Table 2 summarizes the logarithmic mass bins of $\log M_{\text{flip}}$ determined through the KS test according to our new definition for all of the different cases of the web type and R_f considered for both of the $\nu\Lambda\text{CDM}$ models. It also lists the logarithmic mass bins of $\log M_{\text{flip}}^{\text{old}}$ for comparison, where $M_{\text{flip}}^{\text{old}}$ denotes the threshold mass for the occurrence of the halo spin flip defined in the conventional way using the criterion of $\langle \cos \theta_3 \rangle = 0.5$.

3. Discussion and Conclusion

Analyzing the numerical data from the **MassiveNuS** (Liu et al. 2018) and exploring the intrinsic spin alignments of the galactic halos with the eigenvectors of the local tidal fields for $\nu\Lambda\text{CDM}$ models that share the same initial conditions other than $\sum m_\nu$, we have detected a clear trend that in the presence of more massive neutrinos, the spin flip occurs at a lower mass scale. The trend has been found to be the most prominent in the filaments, being robust against the scale variation. We interpret the detected $\sum m_\nu$ -dependence of M_{flip} as an evidence for a retarding effect of massive neutrinos on the nonlinear evolution of the tidal eigen directions.

While in the proto-galactic regime $\hat{\mathbf{J}}$ is aligned with $\hat{\mathbf{e}}_2$ of the linear tidal field (Lee & Pen 2000; Motloch et al. 2020), the nonlinear evolution of the tidal field drives $\hat{\mathbf{J}}$ to develop its alignment with $\hat{\mathbf{e}}_3$ (Hahn et al. 2007b; Libeskind et al. 2013; Lee 2019). The threshold mass for the occurrence of the halo spin flip, M_{flip} , marks the mass scale at which the strength of the nonlinearly developed $\hat{\mathbf{J}}\text{-}\hat{\mathbf{e}}_3$ alignments overtakes that of the initially induced $\hat{\mathbf{J}}\text{-}\hat{\mathbf{e}}_2$ alignments. The faster the tidal fields evolve, the larger the value of M_{flip} is. The presence of more massive neutrinos which exerts stronger suppression of the density growths also retards more severely the nonlinear modification of the tidal eigenvectors from the initial principal directions, leading the galactic halos to retain better the initial memory of the $\hat{\mathbf{J}}\text{-}\hat{\mathbf{e}}_2$ alignments even in the mildly nonlinear regime, and consequently rendering the spin flip to occur at a lower mass scale. Our result reveals the potential of M_{flip} as a new probe of $\sum m_\nu$ on the galactic halo scales, which can complement the conventional probes on the cluster halo scales.

It is, however, worth discussing two limitations of the current analysis and how to

improve them in the future prior to using this new probe in practice. First, the current analysis has not taken into account the fact that the spin directions of the luminous galaxies are misaligned with those of the host DM halos (e.g., Hahn et al. 2010). Given that the galaxies exhibit a different tendency and strength of the spin alignments with the large-scale structures from those of their hosting DM halos (e.g., Dubois et al. 2014; Codis et al. 2018; Ganeshiah Veena et al. 2019; Kraljic et al. 2020), it will be of critical importance to investigate whether or not the luminous galaxies also show the same degree of the $\sum m_\nu$ -dependence of M_{flip} by using hydrodynamics simulations performed for $\nu\Lambda\text{CDM}$ models.

Second, our finding of the $\sum m_\nu$ -dependence of M_{flip} has been obtained from the simulations that includes the relic neutrinos only at the level of the background, which implies that this new probe may not be free from the long-standing σ_8 - $\sum m_\nu$ degeneracy. Although the $\nu\Lambda\text{CDM}$ model with $\sum m_\nu = 0.6\text{ eV}$ has the same amplitude of the primordial power spectra, A_s , as the ΛCDM cosmology with massless neutrinos, they differ in the derived values of σ_8 (Table 1), which should be at least partially contributed to their differences in M_{flip} . A more comprehensive study based on a simulation that incorporates nonlinearly the relic neutrinos (Zhu et al. 2014) will be required to investigate if and how M_{flip} truly varies with $\sum m_\nu$ on the nonlinear scales and to determine whether or not the $\sum m_\nu$ -dependence of M_{flip} can break the σ_8 - $\sum m_\nu$ degeneracy. Our future work will be in this direction.

We thank an anonymous referee for providing us very helpful suggestions. We thank the Columbia Lensing group for making their suite of simulated maps available at the website (<http://columbialensing.org>), and NSF for supporting the creation of those maps through grant AST-1210877 and XSEDE allocation AST-140041. We thank the New Mexico State University (USA) and Instituto de Astrofísica de Andalucía CSIC (Spain) for hosting the Skies & Universes site for cosmological simulation products. We thank J.Liu for providing us with the snapshot data. We also thank the Lorentz Center of the Leiden University for the hospitality during the "Cosmic Web in the Local Universe" workshop where this work was initiated. J.L. and S.R. acknowledge the support by Basic Science Research Program through the National Research Foundation (NRF) of Korea funded by the Ministry of Education (No.2019R1A2C1083855) and also by a research grant from the NRF to the Center for Galaxy Evolution Research (No.2017R1A5A1070354). NIL acknowledges financial support of the Project IDEXLYON at the University of Lyon under the Investments for the Future Program (ANR-16-IDEX-0005). NIL also acknowledges support from the joint Sino-German DFG research Project "The Cosmic Web and its impact on galaxy formation and alignment" (DFG-LI 2015/5-1).

REFERENCES

- Aihara, H., Allende Prieto, C., An, D., et al. 2011, *ApJS*, 193, 29
- Aragón-Calvo, M. A., van de Weygaert, R., Jones, B. J. T., et al. 2007, *ApJ*, 655, L5
- Aragon-Calvo, M. A., & Yang, L. F. 2014, *MNRAS*, 440, L46
- Baldi, M., Villaescusa-Navarro, F., Viel, M., et al. 2014, *MNRAS*, 440, 75
- Behroozi, P. S., Wechsler, R. H., & Wu, H.-Y. 2013, *ApJ*, 762, 109
- Bellomo, N., Bellini, E., Hu, B., et al. 2017, *JCAP*, 2017, 043
- Blue Bird, J., Davis, J., Lubner, N., et al. 2019, arXiv e-prints, arXiv:1912.01062
- Bond, J. R., Efstathiou, G., & Silk, J. 1980, *Phys. Rev. Lett.*, 45, 1980
- Bond, J. R., Kofman, L., & Pogosyan, D. 1996, *Nature*, 380, 603
- Bryant, J. J., Owers, M. S., Robotham, A. S. G., et al. 2015, *MNRAS*, 447, 2857
- Codis, S., Pichon, C., Devriendt, J., et al. 2012, *MNRAS*, 427, 3320
- Codis, S., Gavazzi, R., Dubois, Y., et al. 2015, *MNRAS*, 448, 3391
- Codis, S., Pichon, C., & Pogosyan, D. 2015, *MNRAS*, 452, 3369
- Codis, S., Jindal, A., Chisari, N. E., et al. 2018, *MNRAS*, 481, 4753
- Dubois, Y., Pichon, C., Welker, C., et al. 2014, *MNRAS*, 444, 1453
- Forero-Romero, J. E., Contreras, S., & Padilla, N. 2014, *MNRAS*, 443, 1090
- Ganeshaiah Veena, P., Cautun, M., van de Weygaert, R., et al. 2018, *MNRAS*, 481, 414
- Ganeshaiah Veena, P., Cautun, M., Tempel, E., et al. 2019, *MNRAS*, 487, 1607
- Gonzalez-Garcia, M. C., & Maltoni, M. 2008, *Phys. Rep.*, 460, 1
- Hahn, O., Porciani, C., Carollo, C. M., et al. 2007, *MNRAS*, 375, 489
- Hahn, O., Carollo, C. M., Porciani, C., et al. 2007, *MNRAS*, 381, 41
- Hahn, O., Teyssier, R., & Carollo, C. M. 2010, *MNRAS*, 405, 274
- Hirv, A., Pelt, J., Saar, E., et al. 2017, *A&A*, 599, A31

- Jibrail, A. W., Elahi, P. J., & Lewis, G. F. 2020, MNRAS, 492, 2369
- Kraljic, K., Davé, R., & Pichon, C. 2020, MNRAS, 493, 362
- Krolewski, A., Ho, S., Chen, Y.-C., et al. 2019, ApJ, 876, 52
- Laigle, C., Pichon, C., Codis, S., et al. 2015, MNRAS, 446, 2744
- Lee, J. 2019, ApJ, 872, 37
- Lee, J., Kim, S., & Rey, S.-C. 2018, ApJ, 860, 127
- Lee, J., & Pen, U.-L. 2000, ApJ, 532, L5
- Lee, J., & Pen, U.-L. 2001, ApJ, 555, 106
- Lesgourgues, J., & Pastor, S. 2006, Phys. Rep., 429, 307
- Lesgourgues, J., & Pastor, S. 2012, Adv. High Energy Phys. 2012, 608515
- Lesgourgues, J., & Pastor, S. 2014, New Journal of Physics, 16, 065002
- Libeskind, N. I., Hoffman, Y., Forero-Romero, J., et al. 2013, MNRAS, 428, 2489
- Liu, J., Bird, S., Zorrilla Matilla, J. M., et al. 2018, JCAP, 2018, 049
- Lovell, M. R., Eke, V., Frenk, C. S., et al. 2012, MNRAS, 420, 2318
- Motloch, P., Yu, H.-R., Pen, U.-L., et al. 2020, arXiv e-prints, arXiv:2003.04800
- Pahwa, I., Libeskind, N. I., Tempel, E., et al. 2016, MNRAS, 457, 695
- Paz, D. J., Stasyszyn, F., & Padilla, N. D. 2008, MNRAS, 389, 1127
- Planck Collaboration, Aghanim, N., Akrami, Y., et al. 2018, arXiv e-prints, arXiv:1807.06209
- Pogosyan, D. Y., & Starobinsky, A. A. 1993, MNRAS, 265, 507
- Pogosyan, D. Y., & Starobinsky, A. A. 1995, ApJ, 447, 465
- Ryu, S., & Lee, J. 2020, ApJ, 894, 65
- Tempel, E., & Libeskind, N. I. 2013, ApJ, 775, L42
- Tempel, E., Stoica, R. S., & Saar, E. 2013, MNRAS, 428, 1827
- Trowland, H. E., Lewis, G. F., & Bland-Hawthorn, J. 2013, ApJ, 762, 72

- Vera-Ciro, C. A., et al. 2011, MNRAS, 416, 1377
- Wang, P., Guo, Q., Kang, X., et al. 2018, ApJ, 866, 138
- Wang, P., & Kang, X. 2018, MNRAS, 473, 1562
- Welker, C., Devriendt, J., Dubois, Y., et al. 2014, MNRAS, 445, L46
- Welker, C., Bland-Hawthorn, J., Van de Sande, J., et al. 2020, MNRAS, 491, 2864
- White, S. D. M. 1984, ApJ, 286, 38
- Zhu, H.-M., Pen, U.-L., Chen, X., et al. 2014, Phys. Rev. Lett., 113, 131301

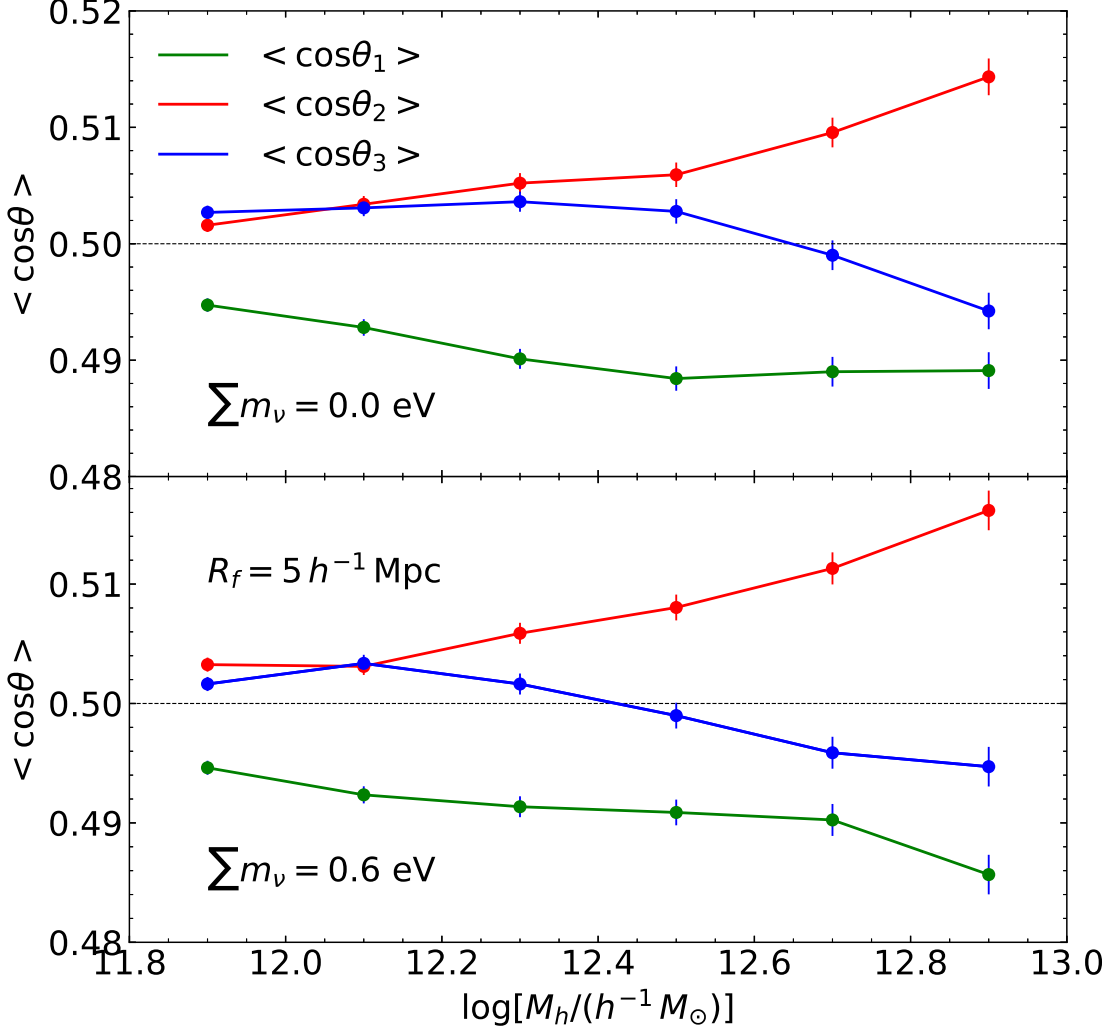


Fig. 1.— Mean values of the cosines of the angles between the halo spin vectors and each of three eigenvectors of the local tidal field smoothed on the scale of $R_f = 5 h^{-1} \text{ Mpc}$ as a function of the halo mass M_h for two different cases of the total neutrino mass $\sum m_\nu$. The dotted line in each panel corresponds to the case of random spin orientations, $\langle \cos \theta_i \rangle = 0.5$.

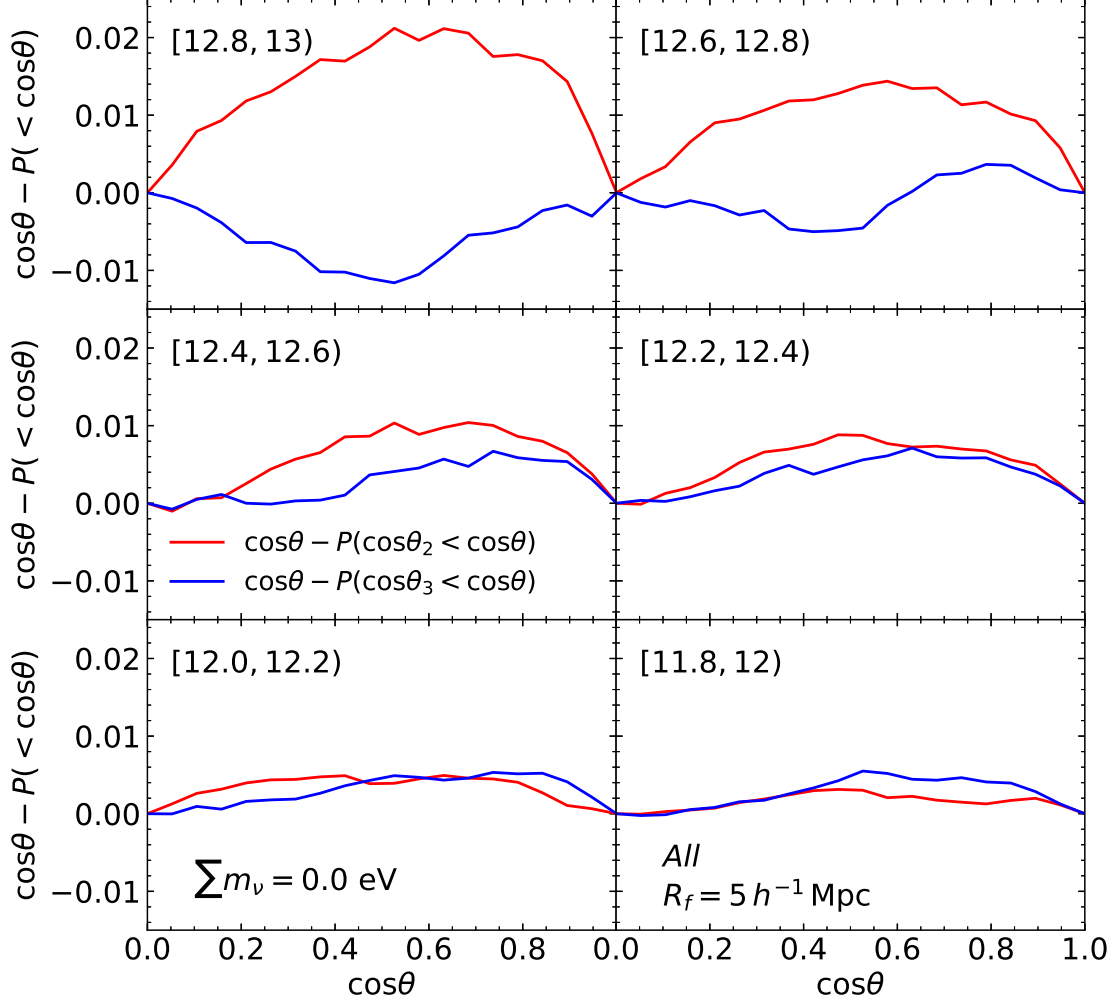


Fig. 2.— Differences between $\cos\theta$ and $P(\cos\theta_i < \cos\theta)$ with $i \in \{2, 3\}$ for the case of $\sum m_\nu = 0.0 \text{ eV}$ at six different logarithmic mass bins of $12.8 \leq \log M_h < 13$, $12.6 \leq \log M_h < 12.8$, $12.4 \leq \log M_h < 12.6$, $12.2 \leq \log M_h < 12.4$, $12.0 \leq \log M_h < 12.2$, $11.8 \leq \log M_h < 12.0$ in the top-left, top-right, middle-left, middle-right, bottom-left, and bottom-right panels, respectively.

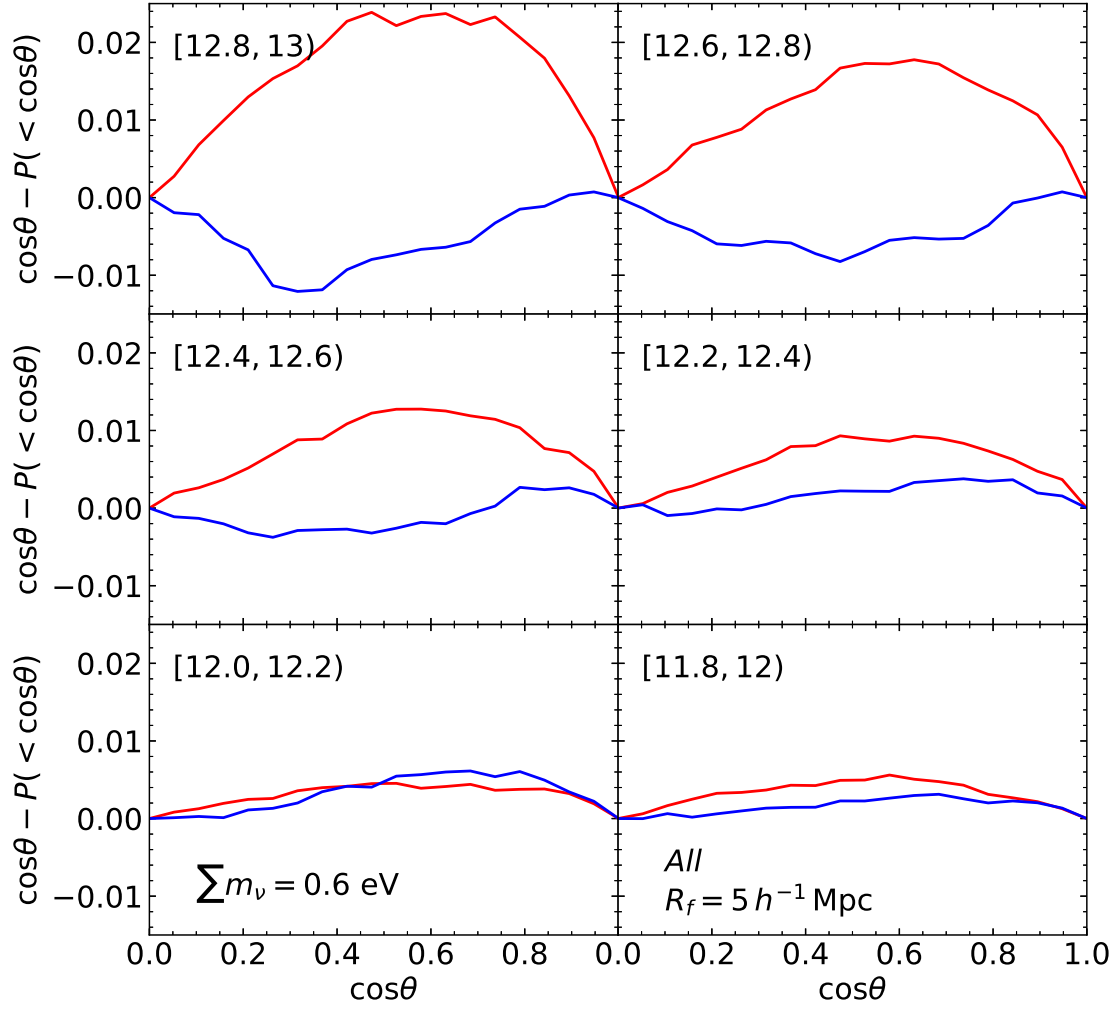


Fig. 3.— Same as Figure 3 but for the case of $\Sigma m_\nu = 0.6$ eV.

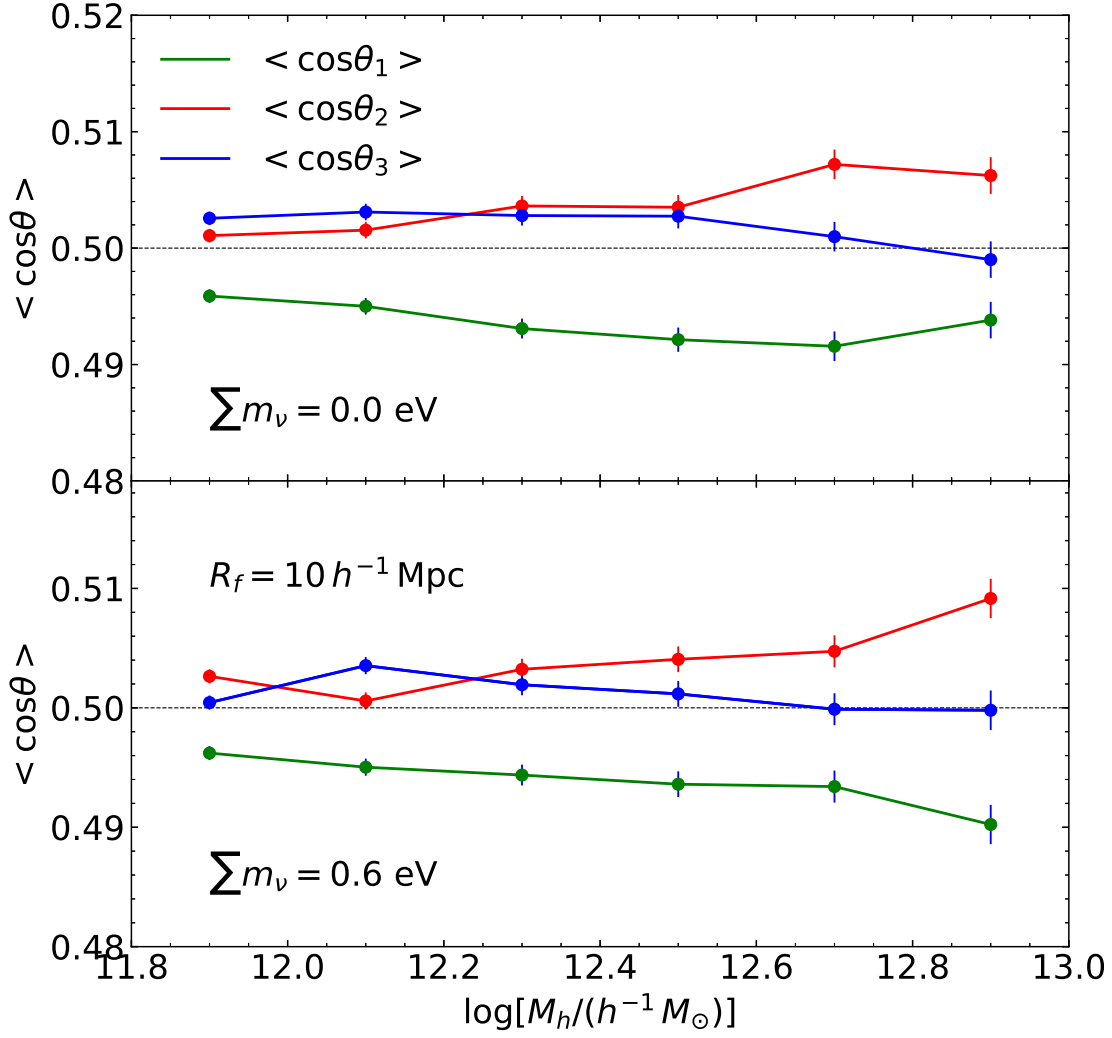


Fig. 4.— Same as Figure 1 but on the scale of $R_f = 10 h^{-1} \text{Mpc}$.

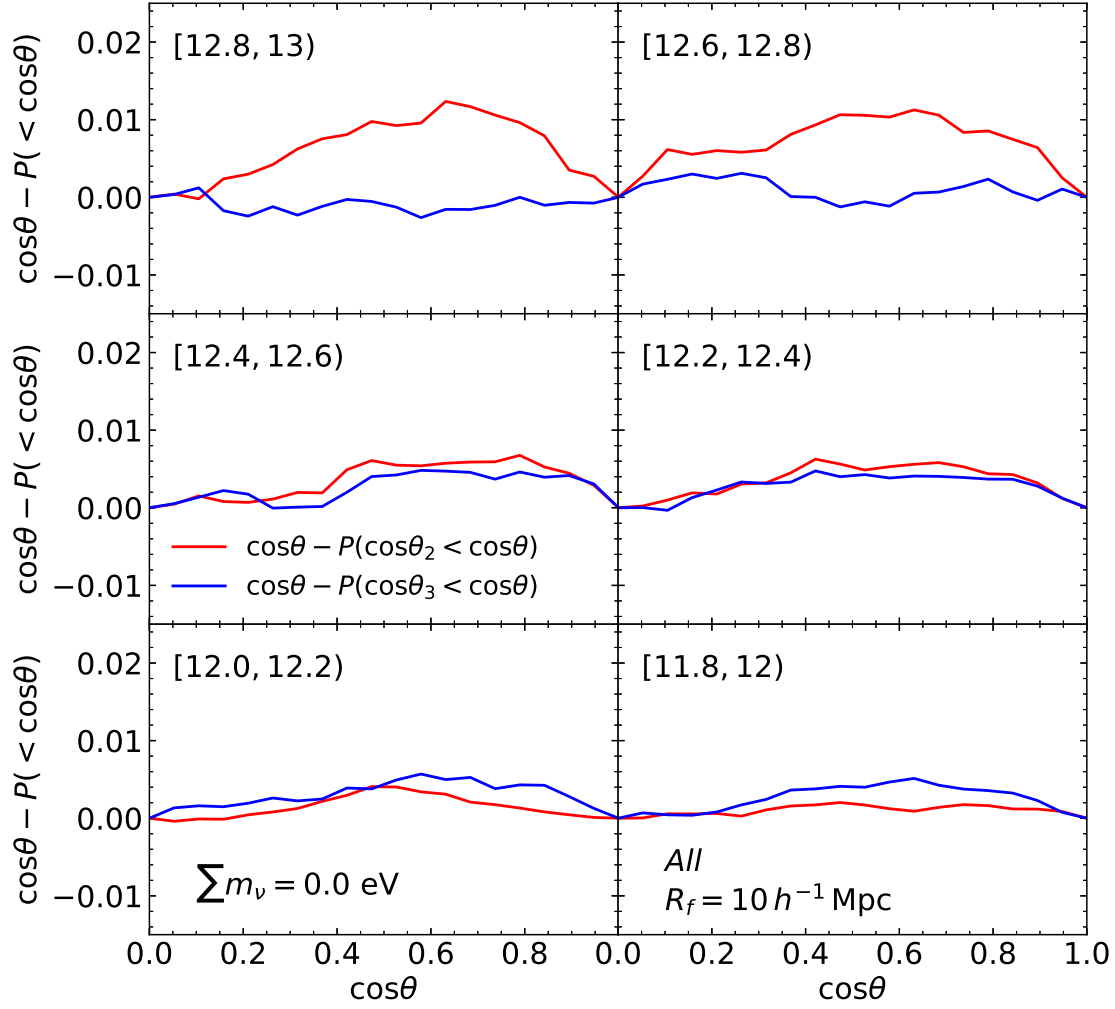


Fig. 5.— Same as Figure 2 but on the scale of $R_f = 10 h^{-1} \text{ Mpc}$.

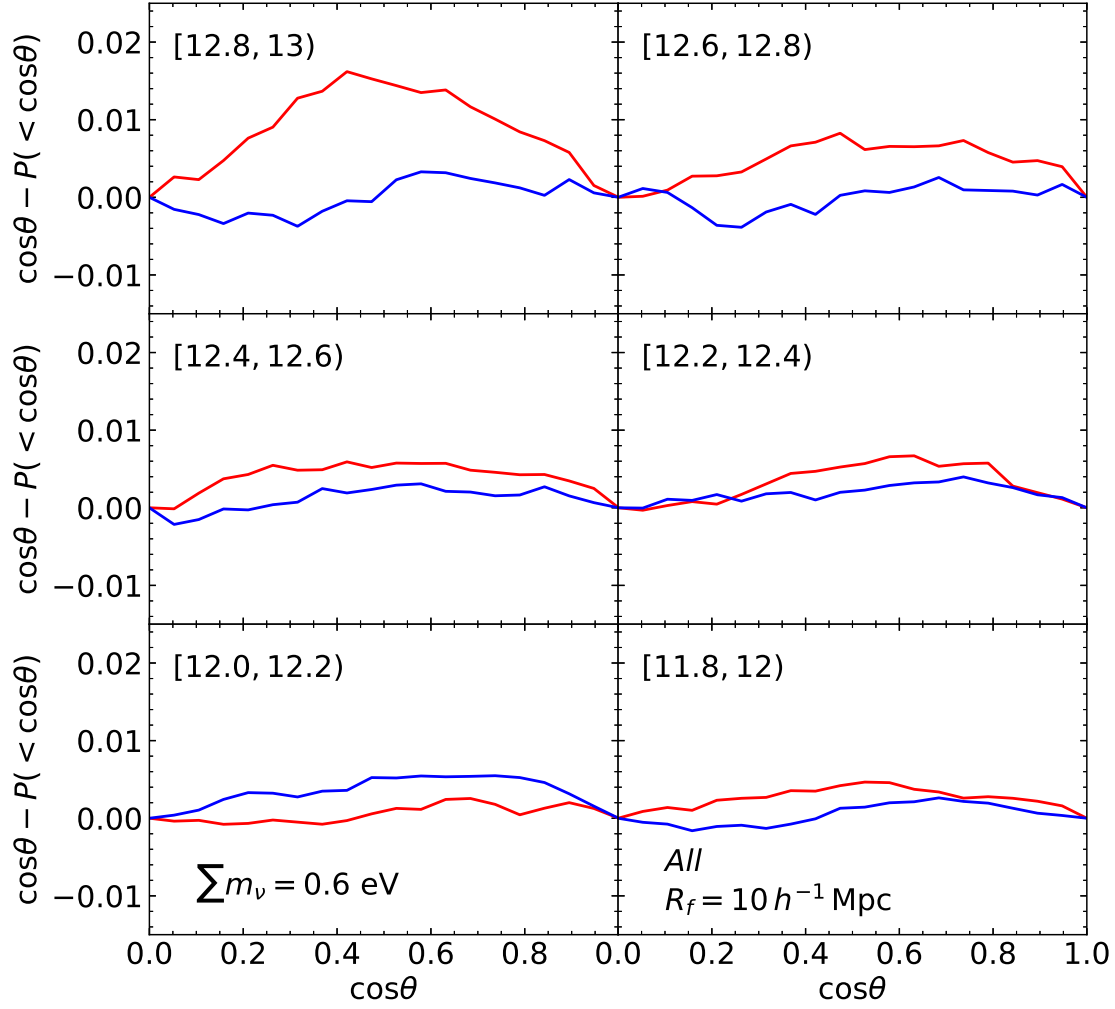


Fig. 6.— Same as Figure 3 but on the scale of $R_f = 10 h^{-1} \text{Mpc}$.

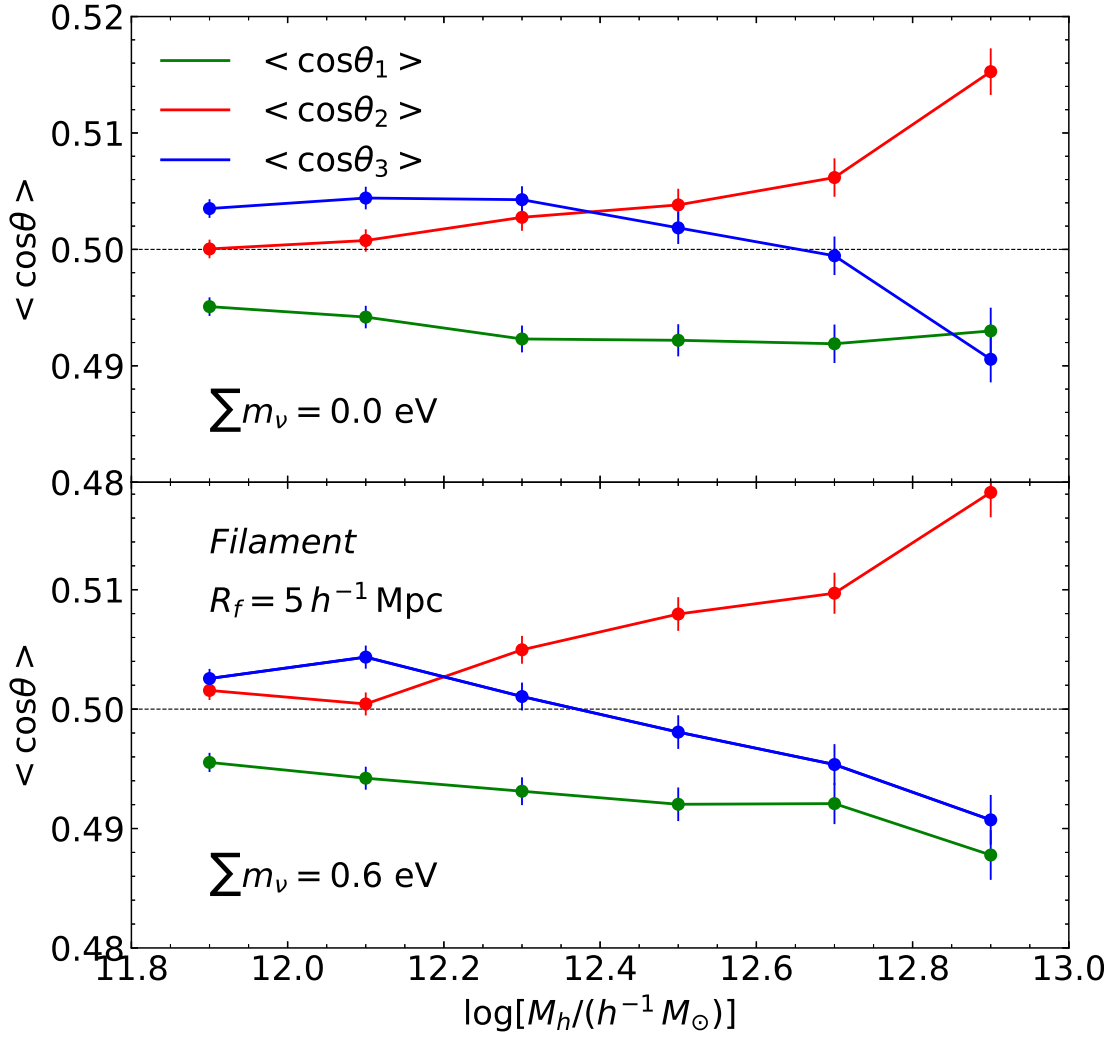


Fig. 7.— Same as Figure 1 but in the filament environment.

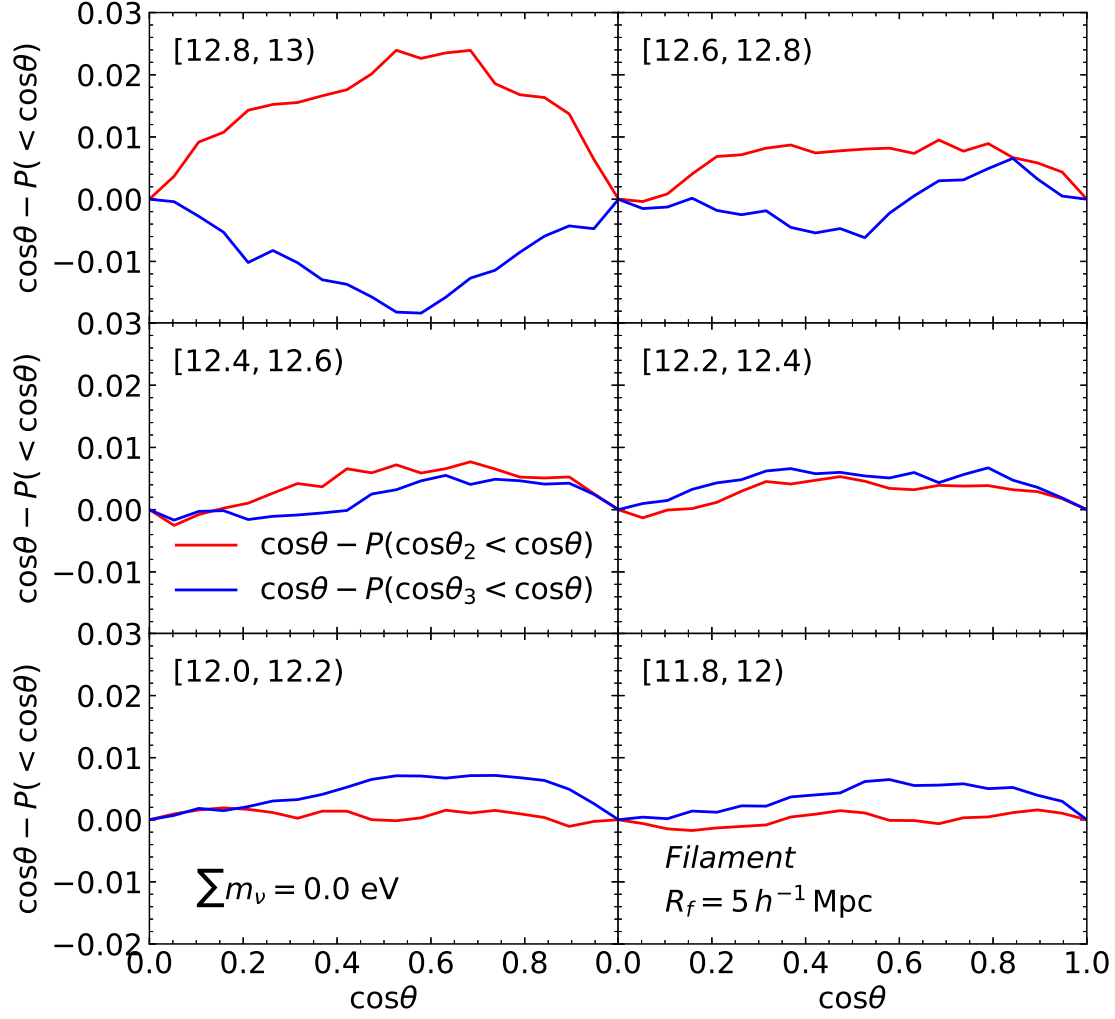


Fig. 8.— Same as Figure 2 but in the filament environment.

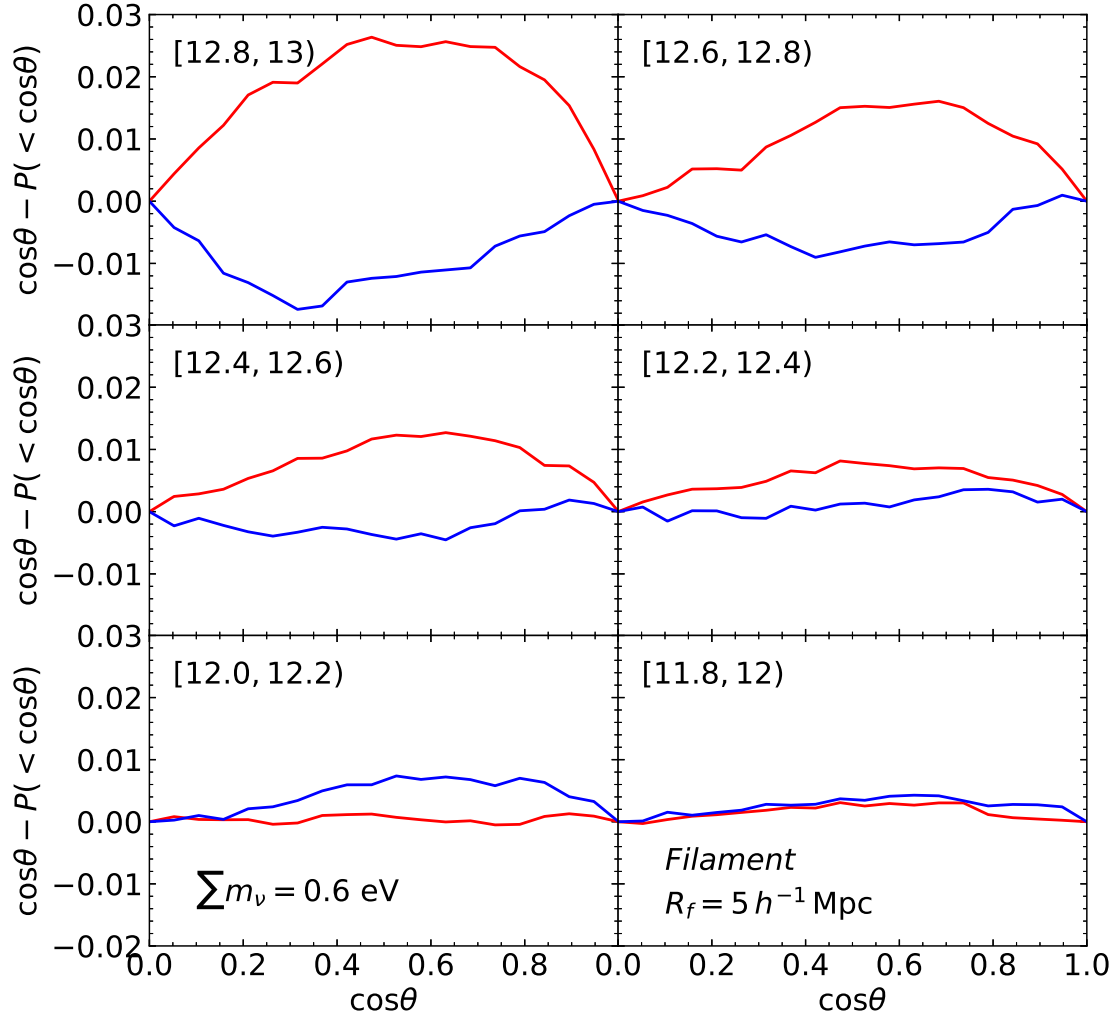


Fig. 9.— Same as Figure 3 but in the filament environment.

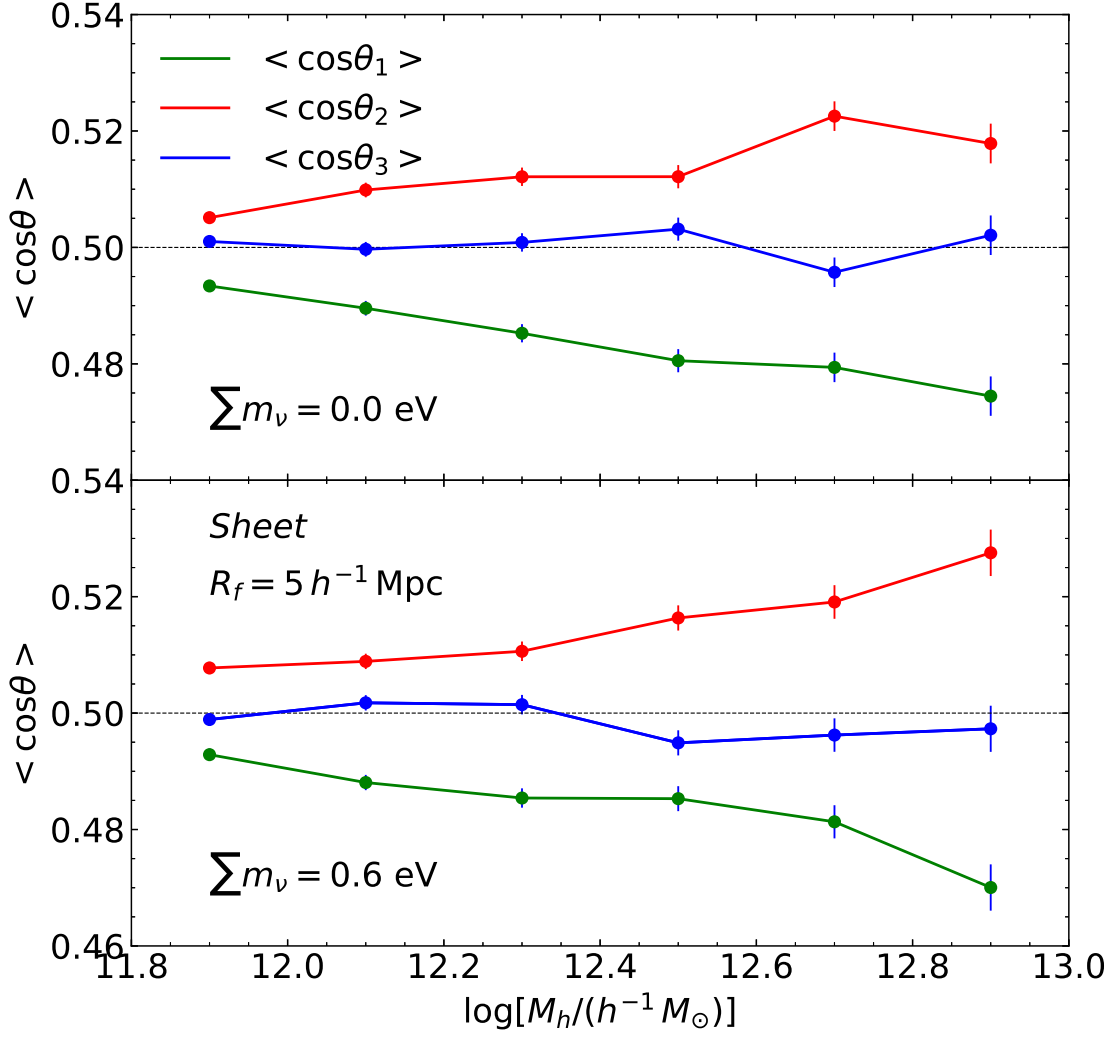


Fig. 10.— Same as Figure 1 but in the sheet environment.

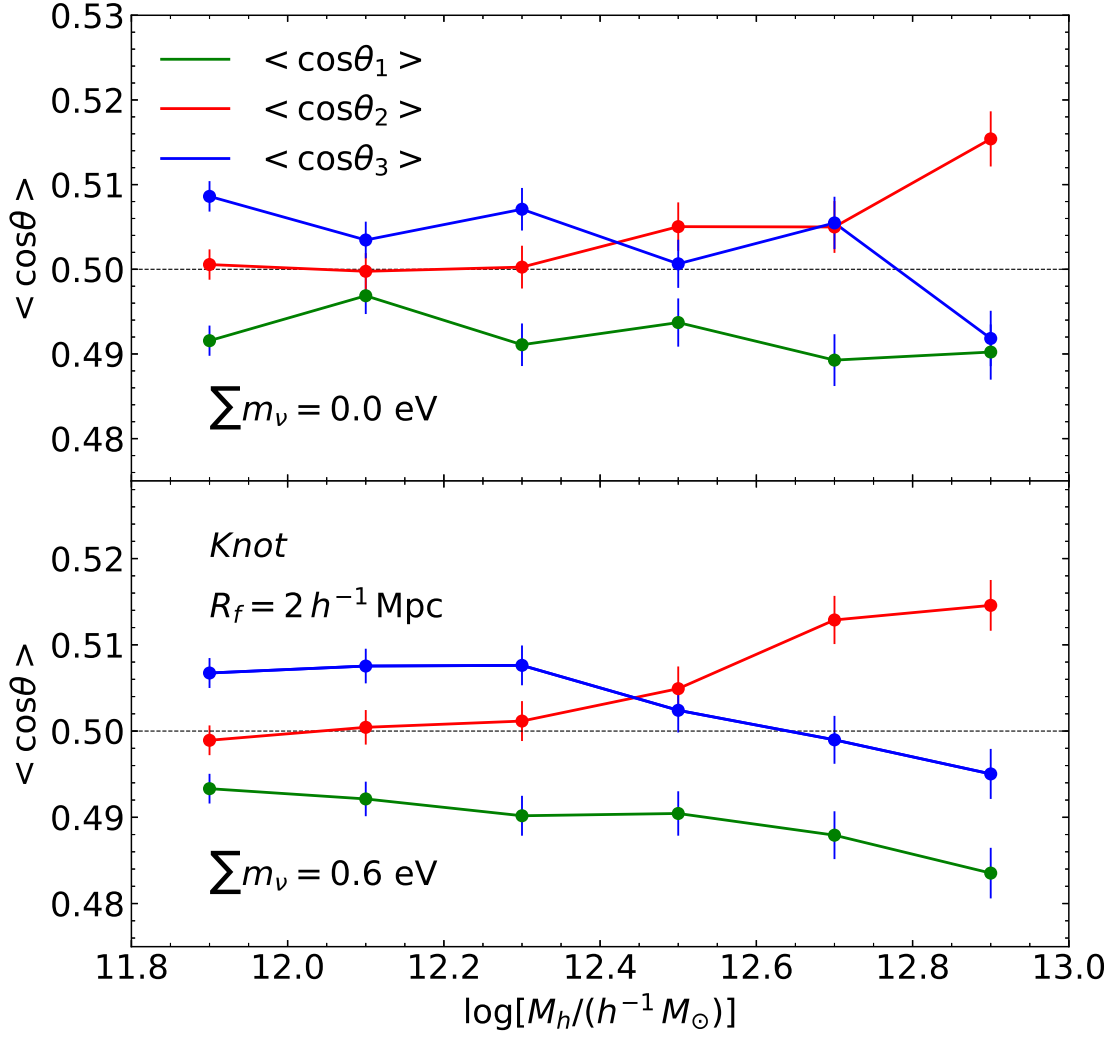


Fig. 11.— Same as Figure 7 but in the knot environment on the scale of $R_f = 2 h^{-1} \text{ Mpc}$.

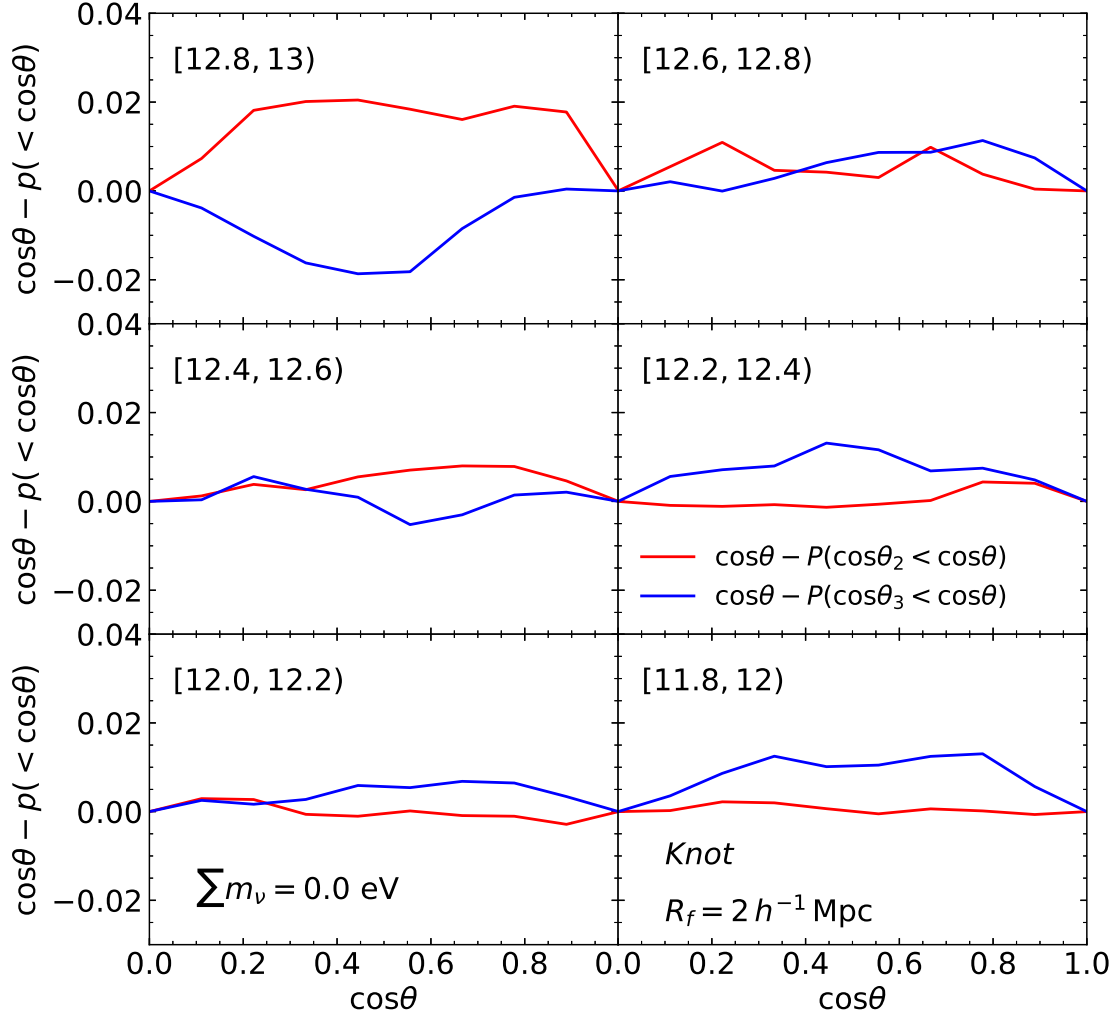


Fig. 12.— Same as Figure 8 but in the knot environment on the scale of $R_f = 2 h^{-1} \text{ Mpc}$.

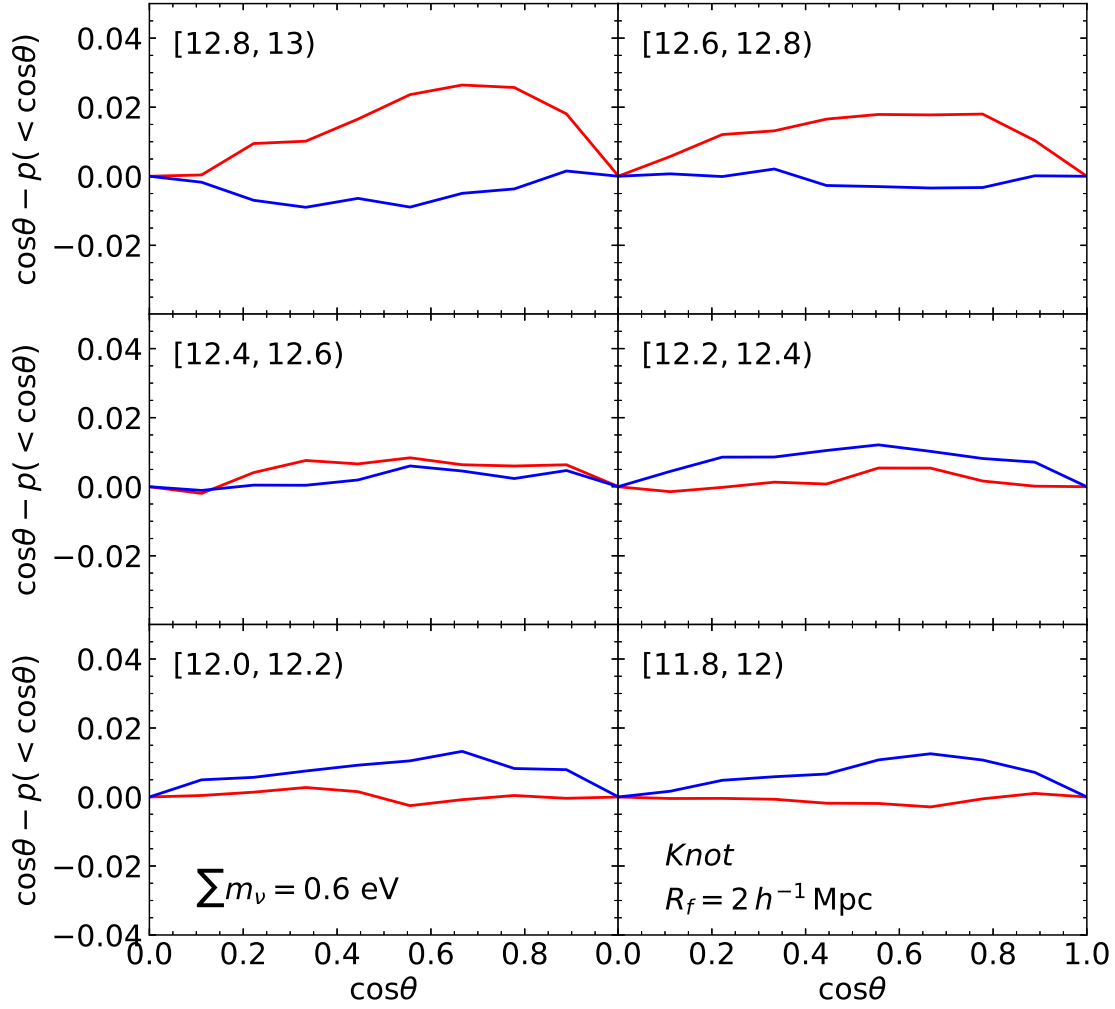


Fig. 13.— Same as Figure 12 but for the case of $\sum m_\nu = 0.6 \text{ eV}$.

Table 1. Initial conditions and the abundance of the galactic halos

$\sum m_\nu$ [eV]	Ω_m	Ω_b	h	n_s	A_s [10^{-9}]	σ_8	N_g
0.0	0.3	0.046	0.7	0.97	2.1	0.85	689654
0.1	0.3	0.046	0.7	0.97	2.1	0.83	680649
0.6	0.3	0.046	0.7	0.97	2.1	0.74	661030

Table 2.

$\sum m_\nu$ [eV]	web type	R_f [$h^{-1}\text{Mpc}$]	$\log(M_{\text{flip}}/h^{-1}M_\odot)$	$\log(M_{\text{flip}}^{\text{old}}/h^{-1}M_\odot)$
0.0	all	5	[12.2, 12.4]	[12.6, 12.8]
0.6	all	5	[12.0, 12.2]	[12.4, 12.6]
0.0	all	10	[12.4, 12.6]	[12.6, 12.8]
0.6	all	10	[12.2, 12.4]	[12.6, 12.8]
0.0	filament	5	[12.4, 12.6]	[12.6, 12.8]
0.6	filament	5	[12.0, 12.2]	[12.2, 12.4]
0.0	knot	2	[12.6, 12.8]	[12.6, 12.8]
0.6	knot	2	[12.4, 12.6]	[12.6, 12.8]